



ELSEVIER

Comput. Methods Appl. Mech. Engrg. 172 (1999) 273–291

**Computer methods
in applied
mechanics and
engineering**

Automated modeling for complex woven mesostructures

R. Wentorf, R. Collar, M.S. Shephard, J. Fish*

*Rensselaer Polytechnic Institute, Department of Civil Engineering and Scientific Computation Research,
4042 Johnson Engineering Center, Troy, NY 12180-3590, USA*

Received 4 May 1998

Abstract

Computational methods for modeling complex three-dimensional woven structures are reviewed and software tools for automated model construction are described. The tools make use of image processing, geometric and attribute modeling, automated discretization, and efficient solvers. The discretization techniques control mesh periodicity and volume fraction errors of meshed constituents due to approximation of curved boundaries. Numerical examples for several woven structures are demonstrated in the context of linear elasticity. © 1999 Elsevier Science S.A. All rights reserved.

1. Introduction

This paper reviews the computational models and emphasizes the modeling tools which assist in the automatic extraction, construction and linking of model geometry and attributes, and automatically produce matched meshes and the associated boundary conditions for analysis of representative volume elements (RVEs) by the finite element method. The techniques can be applied at the scale of weaves or to smaller scale geometries for critical/non-periodic regions needed by multi-scale techniques [15]. These tools include image processing tools, geometric and attribute modeling based on a feature description, automated matched mesh generation, and constituent mesh volume fraction adjustment.

Analysis and design of complex woven architectures at the small scales of the materials has been made both possible and necessary due to advances in composite fabrication, automated meshing and efficient solution techniques. Complex weaves provide the tailored constitutive thermal and mechanical properties for composites used in aerospace and energy conversion. Three-dimensional finite element models of materials at the scale of weaves and fibers can be used to predict linear and nonlinear properties, localized behavior in critical regions of components and are used as a design tool for optimizing composite material design.

The difficulties inherent in generating three-dimensional finite element meshes of geometrically complex domains may be greatly simplified by employing digital image based finite element techniques, as in [20,21]. This method has been shown to provide good results for the homogenized properties, in part because it can capture the correct volume fractions of the constituents, but the poor geometric representation of material interfaces does not directly permit reliable computation of local stresses near constituent boundaries. The approach described in this paper differs in that it maintains a complete representation of the geometric features allowing their influence to be explicitly considered as part of the design process.

The thermal and thermo-mechanical properties of a woven composite were determined in [8] for a plain weave. The discretized model apparently was generated directly from parameters for symmetric/anti-symmetric

*Corresponding author. e-mail: fish@rpi.edu

cases, but no detailed description was given for the modeling and discretization algorithms, especially with respect to their extension to more complicated weave patterns. Other previous work includes a unit cell model used to determine the local stresses in 2-D representations of a woven composite [40]. Geometric modeling capability developed for braids using circular bundles and various approaches for establishing unit cell cutting planes was explored in [32].

This paper is organized into sections reviewing computational models, the development of the RVE model, use of scanned micro-graphs, geometric and attribute model development, the automatic generation of matched meshes, a procedure for controlling the unit cell constituent volume fractions, and the determination of local stress values in the unit cell models. Solver features aimed at efficiently handling poorly conditioned linear systems subject to multiple right hand sides, and the calculation of homogenized stiffness parameters are given in [9].

2. Computational models

In this section we briefly review various modeling approaches for woven composites. A typical shell structure made of multiple layers of woven composites can be modeled on (at least) three different scales: (i) the macroscale (the structural level); (ii) the mesoscale (the weave level); and (iii) the microscale (the level of microconstituents—fibers and matrix within a weave) as shown in Fig. 1. Additional scales can be introduced into the model.

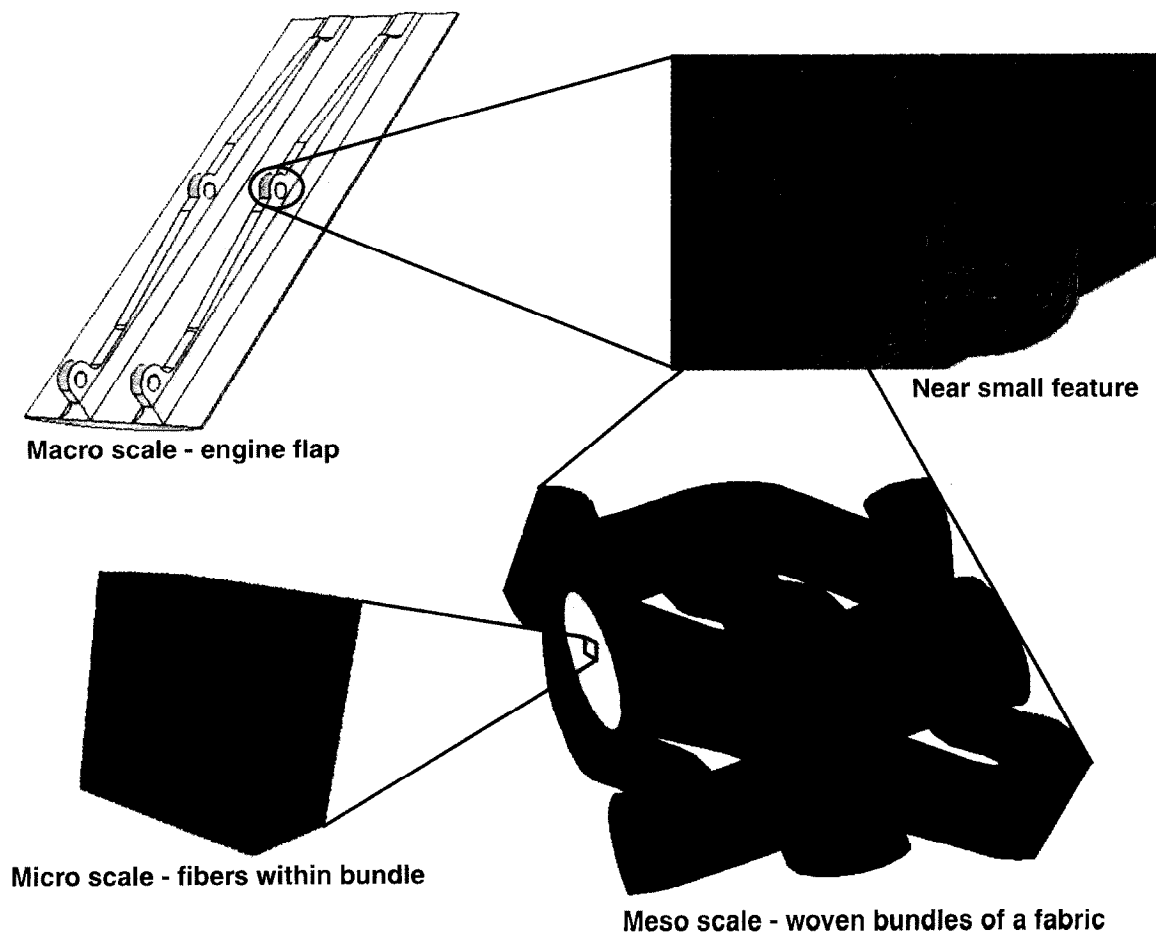


Fig. 1. Multiple scales to be modeled for woven composite components.

For example, the macroscopic scale can be subdivided into two subscales since the thickness of the shell is typically much smaller than its in-plane dimension. Furthermore, the scale of material heterogeneity in each microphase, such as dislocations and grain boundaries could be considered as another scale, not to mention the atomic and electronic scales as the smallest spatial scales.

Computational models can be either deterministic or stochastic. Here we focus on deterministic approaches whereas the insight into stochastic models for composites is given by Babuska and co-workers in this volume. Various deterministic approaches can be classified into the following three categories: (i) the classical uncoupled approach; (ii) the coupled approach assuming micro/meso-structure periodicity; and (iii) the coupled approach free of periodicity assumptions.

2.1. The uncoupled approach

The uncoupled approach employs representative volume elements at one level to produce averaged parameters for the use at the next level. Mathematical homogenization theory [2,5], provides a theoretical framework for the uncoupled approach. For three or more spatial scales mathematical homogenization theory has been employed by Mei and Auriault [27] and Tong and Mey [38].

For woven composite structures, which are idealized as a periodic three-scale medium, a triple scale asymptotic expansion is employed to approximate the solution \mathbf{u} as

$$\mathbf{u}(\mathbf{x}, \mathbf{y}, \mathbf{z}) = \mathbf{u}^0(\mathbf{x}, \mathbf{y}, \mathbf{z}) + \epsilon \mathbf{u}^1(\mathbf{x}, \mathbf{y}, \mathbf{z}) + \epsilon^2 \mathbf{u}^2(\mathbf{x}, \mathbf{y}, \mathbf{z}) \quad (1)$$

where \mathbf{x} , $\mathbf{y} = \epsilon \mathbf{x}$ and $\mathbf{z} = \epsilon \mathbf{y}$ denote position vectors in the macro, meso and micro scales, respectively. The resulting uncoupled governing equations on the macro, meso and micro scales are obtained by inserting the asymptotic expansion (Eq. (1)) into the strong form of the governing equations.

Due to the geometrical simplicity of the microscale problem it is feasible to obtain a microscale solution, consisting of the micro-scale localization tensor, $\mathbf{H}^{\text{micro}}$, and the overall microscale constitutive tensor, $\tilde{\mathbf{L}}^{\text{micro}}$, by means of analytical methods, by exploiting the Eshelby solution of the inclusion problem [28]. The resulting fourth-order tensor, $\tilde{\mathbf{L}}^{\text{micro}}$, provides homogenized material properties for the phases on the meso-scale (average bundle and matrix properties), whereas the third order tensor $\mathbf{H}^{\text{micro}}$ is utilized for postprocessing of local fields on the microscale.

Numerical methods (FEM, BE, PUM) are typically employed for analyzing RVEs of complex woven composite mesostructures. The solution of the mesoscale problem, \mathbf{H}^{meso} and $\tilde{\mathbf{L}}^{\text{meso}}$, is then used for both the postprocessing on the mesoscale and as an input in the form of homogenized material properties to the macroscale problem, respectively. Two examples of such mesoscale post-processing are presented in Fig. 2, where the distribution of maximum principal stresses in the weave are due to an applied load on the macro-scale structure. The macro scale structure was a gas turbine component analyzed with the derived properties, $\tilde{\mathbf{L}}^{\text{meso}}$. The model at the top of the figure shows the bundles of a single layer of a five harness satin weave fabric (the weave repeats after every five warp and five weft bundles), while the bottom three images are an exploded view of the stresses in the warp bundles, matrix, and weft bundles of a trial design which interlocks adjacent fabric layers. The distribution indicates the stress increases due to weave features, such as sharp bends, under linear elastic loadings.

The computational complexity of solving nonlinear heterogeneous systems is much greater. While for linear problems an RVE problem has to be solved only once, for nonlinear history dependent systems it has to be solved at every increment and for each integration point. Moreover, history data has to be updated at a number of integration points equal to the product of integration points at all modeling scales considered. We refer to the paper by Fish and Shek in this volume [19] for presentation of various nonlinear approaches.

2.2. The coupled approach for periodic micro/meso-structures

Recent theoretical and numerical studies conducted at Rensselaer [16] have shown that in the areas of high gradients, primarily developed in the boundary layers at free edges and interfaces, the classical uncoupled approach may lead to poor predictions of local fields, since it assumes uniformity of macroscopic fields over the RVE domain. These findings motivated the development of the coupled multiscale approach.

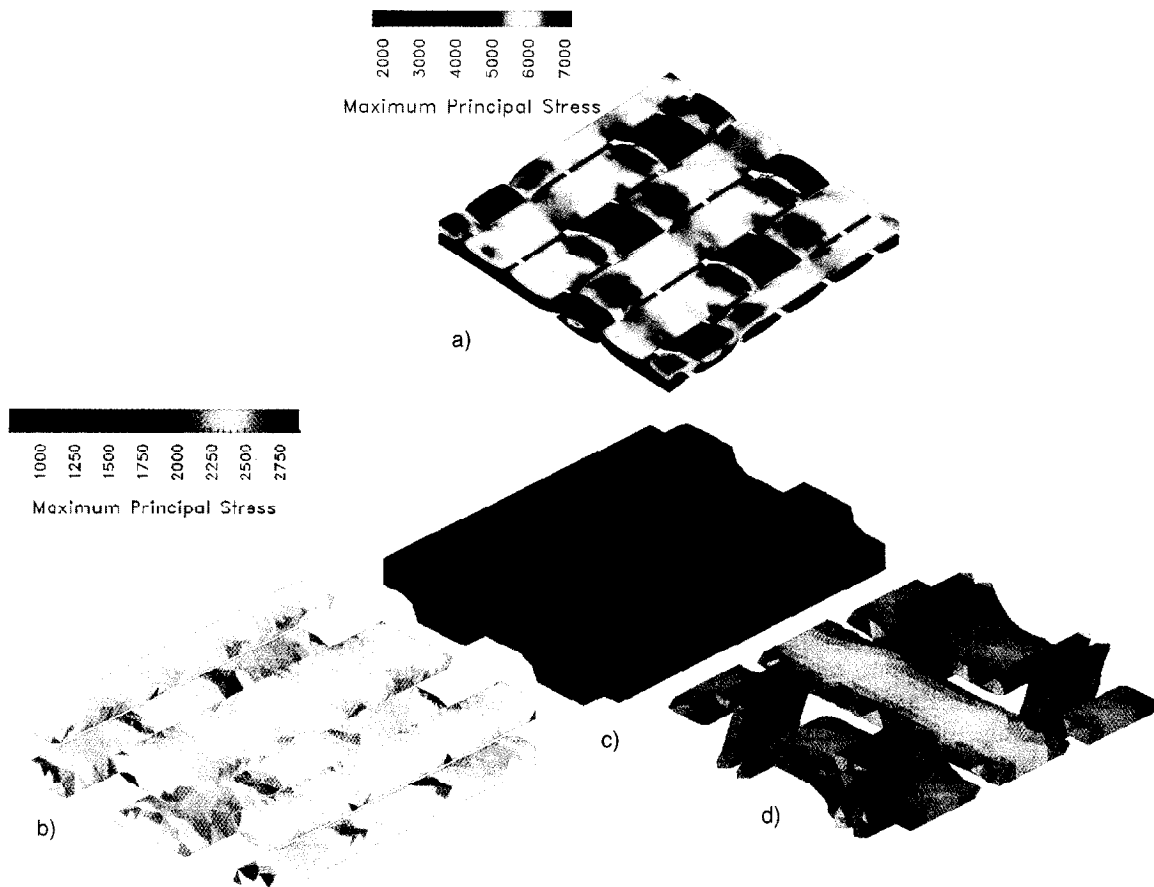


Fig. 2. Computed maximum principal meso scale stresses on the meso scale due to an applied macro scale stress: (a) a five harness satin weave, (b) the warp direction bundles, (c) the matrix, (d) the weft direction bundles of a ply-interlocked weave.

In [14,15] we have shown that the meso-scale model serves as an ideal mechanism for capturing the lower frequency response of the micro-scale model, whereas the lower frequency response of the meso-scale model is accurately represented by the macro-scale model. Therefore, the discrete version of postprocessing operators in the uncoupled approach, $(\mathbf{I} + \mathbf{H}^{\text{micro}} \nabla_s)$ and $(\mathbf{I} + \mathbf{H}^{\text{meso}} \nabla_s)$, can serve as an interscale transfer (or prolongation) operator in the multilevel process [15], where ∇_s is a symmetric gradient operator. The rate of convergence of the resulting multilevel process has been studied in [14].

2.3. The coupled approach for nonperiodic micro/meso-structures

For highly nonperiodic heterogeneous media the *global* interscale transfer operator, which is fixed in space, does not exist due to the spatial variability of the micro/meso-structure. However, if the micro/meso-structure is known (i.e. can be reconstructed from micrographs) it is possible to compute a *local* interscale transfer operator using the Generalized Aggregation Method (GAM) [17,18], or Homogenized Dirichlet Projection Method (HPDM) [30].

Using Generalized Aggregation Method the auxiliary piecewise-constant homogenized model can be constructed from the fine scale model by decomposing the whole set of nodes in the fine scale into non-intersecting blocks to be referred to as aggregates, and then for each aggregate assigning a reduced number of modes based on the local eigenvalue analysis. The resulting piecewise-constant homogenized model effectively captures the lower frequency response of the fine scale model.

For details on the Homogenized Dirichlet Projection Method, see the paper by Oden and co-workers in this volume.

3. Development of a representative volume element model

Three-dimensional weaves are complex assemblies of matrix and fiber bundles, and may also contain cracks and voids in the matrix material. Representative Volume Elements (RVEs) have been defined as the smallest possible volume or ‘building block’ of a composite material which has the same effective properties as would a homogeneous material model at a higher scale, usually that of the whole artifact [8,34]. The modeling process involves the selection of constituent phases and their significant features, the constitutive model(s) and associated property parameters of the solid phases, and the boundary conditions needed for the goals of the analysis. The constitutive model is chosen based upon the material constituents, the environment, loading and expected lifetime and the property parameters that have been measured. The smaller-scale modeling of the fibers within the bundles was supplied via the Mori–Tanaka [28] method for the bundles shown in this paper. Given a complex arrangement of fibers, interfaces coatings and cracks, such as in Fig. 3, a RVE could be developed for the bundles and its homogenized properties used instead. The boundary conditions depend on the formulation of the subsequent analysis.

The constituent geometric features determine the dimensionality of the model and can be given either directly as basic design dimensions, or by scanned specimen data, subject to discretization, noise processing and interpretation parameters. The overall shape of the unit cell is a rectangular prism, although the modeling capability can be used with other shapes. The longest wavelength of a periodic feature controls the size of the unit cell in each direction, still leaving an infinite number of possible cells geometries based on the locations of the cell boundaries in the periodic pattern [32]. In practice, this may be determined by convenience, specifically where there are alternatives in the location of self-intersecting boundaries of periodic faces.

The goal is to provide general modeling and analysis processes: not limited in dimensionality, number of scales, assumptions of symmetries or periodicity, type of weave or number and kinds of features, or analysis goal (property estimation, sensitivity analysis and optimization). The approach is based on development of a non-manifold geometric model, then automatic mesh generation to create a matched mesh with periodic boundary conditions¹, as shown in Fig. 4. Efficient solvers and post-processing capabilities compute results, such as the homogenized stiffness or stress concentrations, which are either the ultimate goal of the analysis or used as input to an optimization. The geometric model provides the connection between design and manufacturing parameters, and the discretized model used by the solver. They enable optimization with respect to the desired set of design/manufacturing parameters.

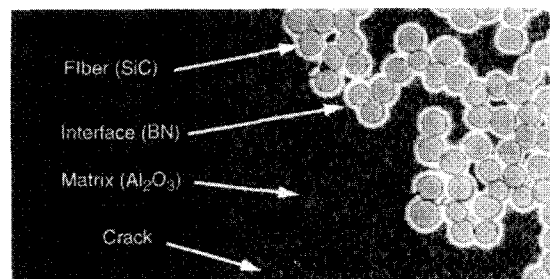


Fig. 3. Fiber scale image [25].

¹Alternative approaches for boundary condition specification have been used by others, but the homogenization analysis used here requires that displacement fields vary identically over opposing faces. Ensuring a matched meshes on selected faces of an RVE is considered to be the governing case in terms of automated modeling complexity.

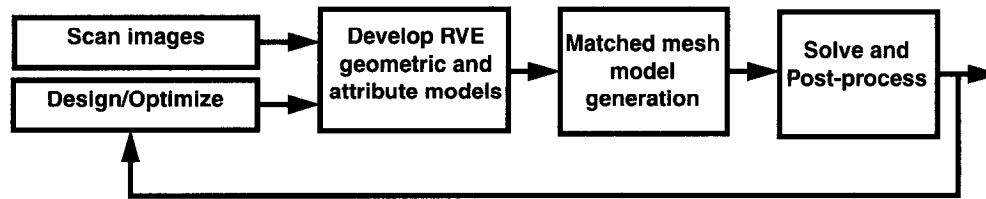


Fig. 4. Schematic of modeling and analysis operations.

3.1. Model development from images

In cases where the composite has been manufactured, model parameters can be obtained from micro-graphs of polished specimens with the aid of image processing software. The images are scanned as grey-scale pixel maps, from which both volume fractions and the centroidal locations of given features are measured. Image features are collections of pixels with similar light intensity, exposed by the polishing of fibers, coatings, bundles, cracks, voids and matrix material. The original pixmaps were produced from photographs scanned with the aid of Photoshop™ [1], and then converted to a PGM format with X-Windows and the XV™ [7] software utilities. Once formatted, the software automatically performs the measurements on given regions of the micrograph, given a range of threshold grey-scale values. Calibration of the threshold ranges was aided by auxiliary software, which plots cumulative volume fraction as a function of increasing threshold ranges. A spreadsheet reads the processed data, organizes and serves the role of constraint propagator [11] and manager weave parameters.

Images at multiple scales are processed, at the weave scale to compute dimensions of a unit cell, bundle and crack/void sizes and positions, and at the fiber scale to find fiber volume fractions within the bundles. Image processing of 3D ‘voxels’ has been used earlier for directly creating discretized unit cell models of bone tissue using brick elements, where the element’s isotropic stiffness was inferred directly from the grey-scale value of the voxels [21]. The high temperature composite ceramic application described here has additional complications, namely:

- the structure consists of multiple distinct phases at each scale, and meso scale images also contain fiber scale features,
- the material is manufactured, requiring the specification of geometry from a small set adjustable design parameters,
- the analysis goals (stiffness and stress concentrations) have different discretization requirements,
- image sources may be limited to 2D polished sections, due to the cost and resolution limitations of voxel imaging,
- specimen preparation methods can add image features and bias the grey-scale values over the field of the image.

An example of the last item is shown in Fig. 5, where polishing of the specimen often cracks and removes the feathered edges of fibers inclined to the polish plane. The resulting black half-ellipses are not voids in the as-processed microstructure. The chipped edge features may be used to infer the direction ($\theta < 90^\circ$ or $\theta > 90^\circ$) of the fibers and the bundle. In addition, if a statistical description of the fiber cross-sections is known, the elongation of the cross-section can be used to estimate the inclination angle θ . The effects of noise and multiple features sharing the same grey-scale value (first issue listed) can be seen in Fig. 6. The image on the right shows the specimen, while the larger image on the left is a magnified view showing the pixels used for a small portion of the specimen. Using only a range of grey-scale or density values to interpret a micro structure over the entire image is problematic because the crack, the cross fiber and imaging noise in the matrix, combined with non-uniform lighting over the image lead to overlapping value ranges. For these situations, automated image processing would require methods to recognize collections of pixels and classify them with respect to features based on size and shape. These types of problems has been researched for purposes of optical character recognition (OCR) [24,31] other applications such as medical image interpretation.

The typical steps involved in OCR are thresholding and noise reduction, then recognition based upon thinning

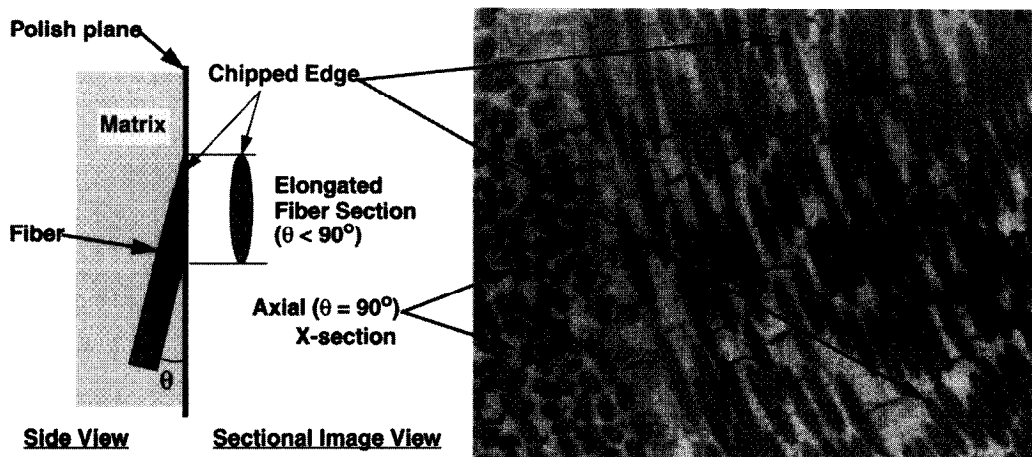


Fig. 5. Some fiber image features [25].

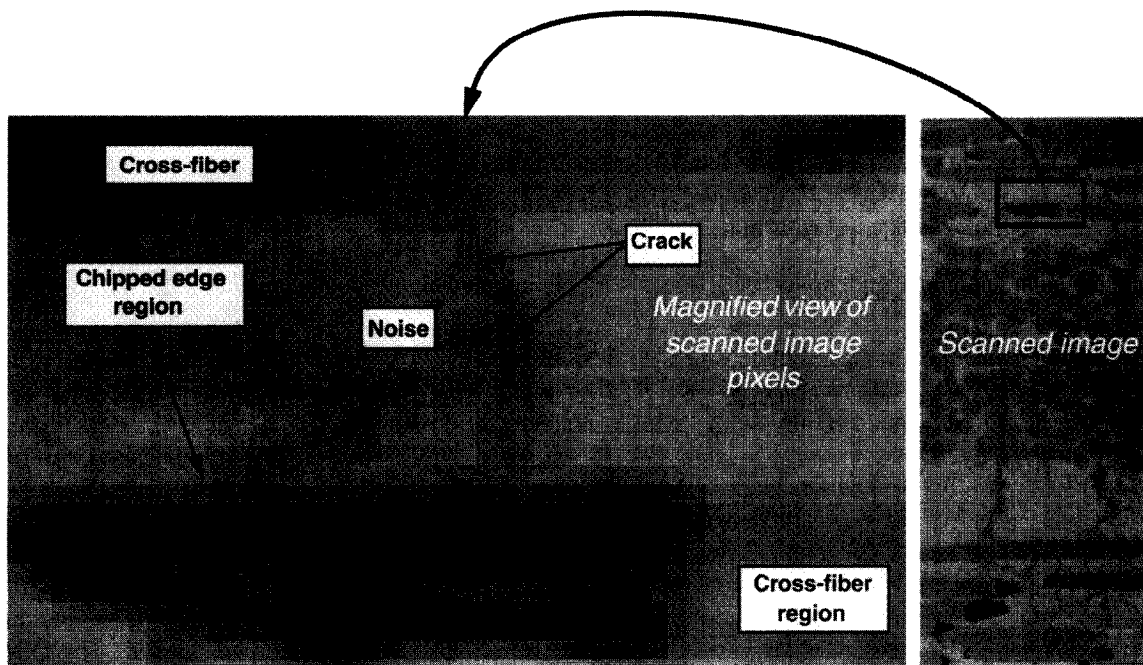


Fig. 6. Pixel map—effects of image noise, discretization, sample preparation [39].

area, perimeter, direction coding, bounding box, thinned arc length, thinned topology, orientation and aspect ratios [31,29].

The feature recognition problem for composite material specimens can be simpler than that of text recognition, since the features are not recognized based on orientation, the feature set is much smaller, and only statistical averages, rather than a series of successful classifications, are needed [6,24,31]. Undesired smaller scale features, e.g. the crack in Fig. 6, are often resolved in the image and would require detection and classification according to size measures and shape measures, such as thinned thickness. Lowering the scanning resolution can eliminate this problem by averaging, but this can also effect the location of the boundary of the desired features. Methods combining both lower and higher resolutions may be useful.

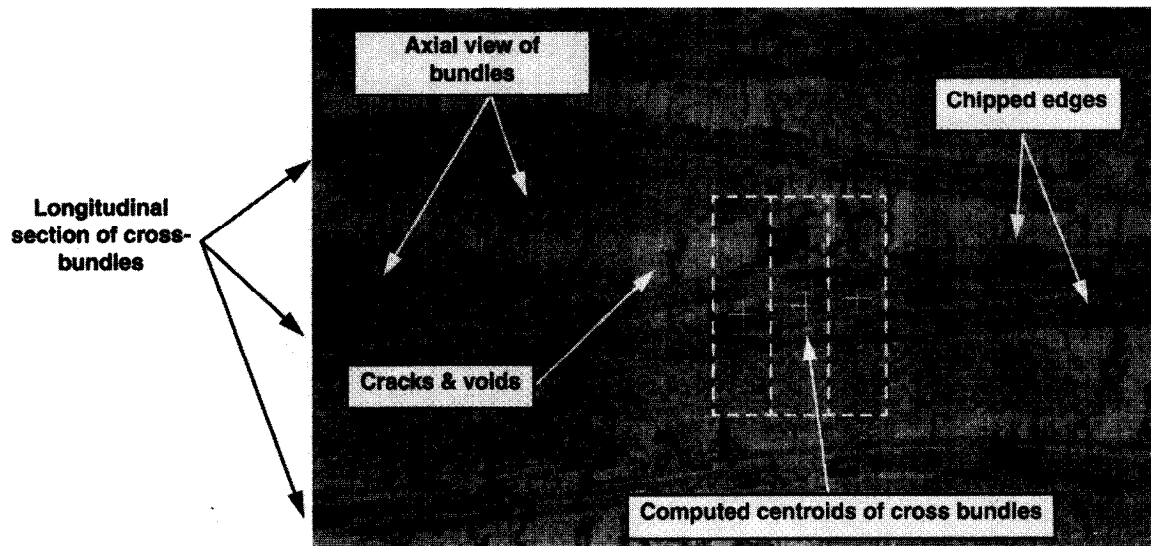


Fig. 7. A 2D weave section and some material features [39].

An example meso scale image is shown in Fig. 7, where the bundles oriented normal to the polish plane are ellipsoidal or flat oval shapes, and the bundles running parallel have chipped edges. Size and center–center spacing parameters were extracted for axial bundles and cracks. By discretizing the cross-bundles into segments (dashed boxes in Fig. 7), classifying the pixels into the matrix, axial and longitudinal fiber regions, and then computing the centroid of longitudinal fibers in each segment, a set of control points are obtained for typical bundle paths as they cross over each other.

3.2. Geometry and attributes

Models for woven composites may be generated from images of test specimens, as described earlier, or from conceptual design specifications. New 3D weave designs are strongly dependent on the capabilities of the particular perform fabricator and are created with a minimum of design data.

An example hand-drawn weave schematic, which can be a typical means of communication for initial designs, is shown in Fig. 8. The schematic, a 2D section cut, depicts the inter-weaving of the bundles, where the bundles directed out of the page are shown as filled dots. The schematics and associated written descriptions must be assembled into a coherent 3D weave topology for the repeatable unit cell, or a suitable unit cell idealization². The weave design specification often includes the ‘volume fraction’ in each direction for each type of bundle, where ‘volume fraction’ indicates the target percentage of fiber cross-sectional area to the total of all specified section areas. Some example bundles types are ‘warp’ and ‘weft’, ‘stitch’ and ‘binder’. The finished component dimensions, such as thickness, and some indirect measure of bundle size, such as ‘denier’ and ‘picks’ per unit length are also usually given. Regions where a ‘stack’ of bundles will contact and be constrained by a component dimension, see Fig. 8, can be used to determine positions of bundle cross-sections within the cell. Development of a descriptive language permitted the variety of given specifications to be resolved into a standardized expression of the weave’s ‘features’ and parameters for subsequent automated modeling.

Software tools assist the conversion of the specifications to the complete description, and automatically convert the description into a sequence of geometric and attribute modeling instructions. The term ‘feature’ is extended from a manufacturing sense to include a grouping of geometric entities for a common analysis purpose or design function [35]. Some examples are the opposite faces of a rectangular unit cell which are to have matching meshes, see Fig. 9, a solid region within the RVE which represents a bundle of fibers, the set of faces,

²Weave patterns may repeat within the relative scale size assumptions of the uncoupled approach or even within the confines of the component.

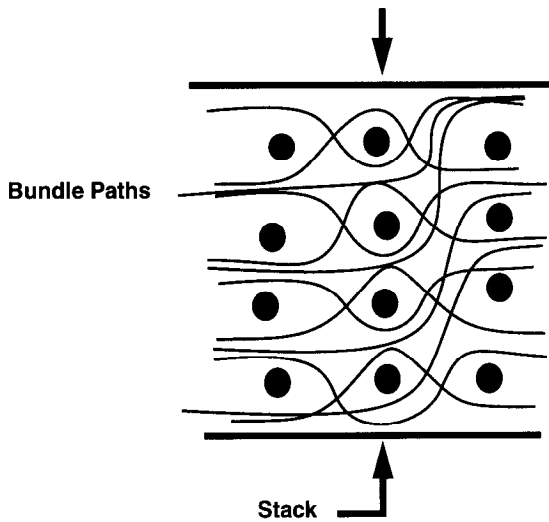


Fig. 8. Part of a typical weave schematic.

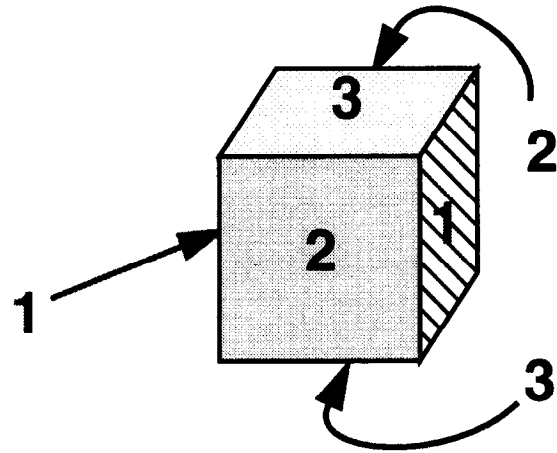


Fig. 9. Matching faces.

edges and vertices in the RVE which are dependent on a design parameter, or the topology of the interacting bundle paths consistent with a type of weave. The feature based approach provides a declarative description of the RVE, i.e. one where the RVE is the combination of each of the set of constituent features. Features are defined by type, size and position parameters, examples of which are shown in Fig. 10. The bundle cross-section type and size parameters are defined as in Fig. 10(a), where the type can be a geometric primitive, such as the ellipse, or an assembly, such as an oval, or if necessary, the two-curve cross-section of Fig. 10(b). The bundle sections are generally idealized as smooth shapes to avoid artificial stress concentrations. Conversion of the feature description to sequential modeler operations can involve the shape and positioning of interacting features, such as the warp and weft woven bundles, and in general requires several modeler operations. The model construction operations are evaluated by a commercial modeler to produce a non-manifold boundary representation (B-rep), in which regions of a constituent are bounded by faces, faces by edges, etc. [26,42,42].

The boundary representation is comprised of both topology, which describes the relationships of the model entities, and geometry or shape, which describes the mapping of the point set of each topological entity onto the Cartesian or real image space of the model. The regions, faces, edges and vertices are each topological entities which encapsulate shape information, direction of outward normals, and the bounding and/or bounded by relationships of the topological entities with one another. The topological entities also provide the data structure on which attributes are attached [4,36].

Several modelers are available to support the underlying construction operations including primitive instantiations, curve fitting, extrude and sweep operations, and Boolean combinations. The commercial non-manifold modeler, SHAPES™ [44] was used here. Example primitives are boxes, cylinders, ellipsoids, their lower dimensional equivalents such as lines and points, all of which are available to model straight fibers, voids, cross-sections or the unit cell domain. Sweep operations, such as extrude or tangent sweep, are also

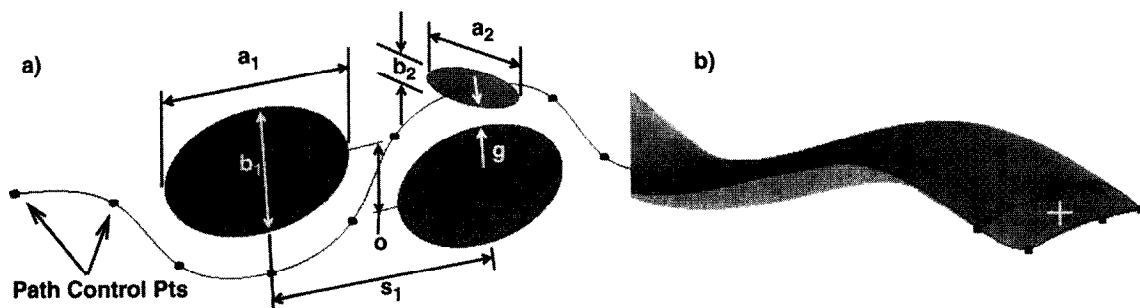


Fig. 10. Bundle sections, (a) ellipsoidal parameters, (b) volume swept from a distorted section.

supported and are typically used to define bundle regions. The modeler also provides constructive solid geometry (CSG) type operations, including the Boolean operators: union, intersection and subtraction, and affine transformations, such as translate, scale and rotate. The CSG operators are typically used to combine the constituents into the final model of the unit cell.

RVEs for complex 3D weaves result in several thousand topological entities, and many times that have been instantiated during the construction operations, thus providing the motivation for efficient automatic attribute identification processes. Attributes include analysis attributes, such as the material properties, matching faces, and essential boundary conditions, as well as the design parameters associated with each topological entity. As described in [36], attributes used in analysis can be represented in the general case as tensors distributed over geometric entities, and organized into hierarchal groupings. For the purposes of automated construction of RVE models from declarations of included features, a method was developed which automatically propagates attributes identifiers, originally assigned to individual features, to the topological entities produced by their combination.

An example of the process is illustrated in Fig. 11, where a CVD coated plain weave model is developed from regions representing the coating, the unit cell template, and the bundles of fibers, model entities *A*, *B*, *C*, respectively. The ancestor values {1, 2, 3} used to track matching faces are indicated for the unit cell template 'B', and are propagated onto faces of both bundle and matrix regions, shown on the right of Fig. 11. As indicated in the lower right, the final configuration can be produced by more that one sequences of Boolean operations. The example illustrates some of the necessary characteristics of the attribute propagation process:

- Support of multiple attribute identifiers per topological entity of arbitrary dimension.
 - Assignment of attribute identifiers based on topological relationships, e.g. assign a debond strength to the set of faces common to regions with dissimilar materials.
 - Consistency throughout arbitrary sequences of Boolean construction operations, satisfying standard set theoretic identities on the point sets of the topological entities: idempotency, commutivity, associativity, distributivity and absorption.
 - Control of propagation, such that attribute identifiers can have precedence. This feature avoids a combinatorial explosion of attribute-topological entity tuples. Fig. 11 shows results of the precedence function: The bundle material attribute identifier take precedence over those of the coating in the volume of overlap.
 - Relational recovery and organization of attributed topological entities for subsequent analysis, e.g. find the set of regions with a given material, list the set of faces associated with a given design parameter, etc.
- To implement automatic propagation of attribute identifiers, 'ancestor tags' are connected with each

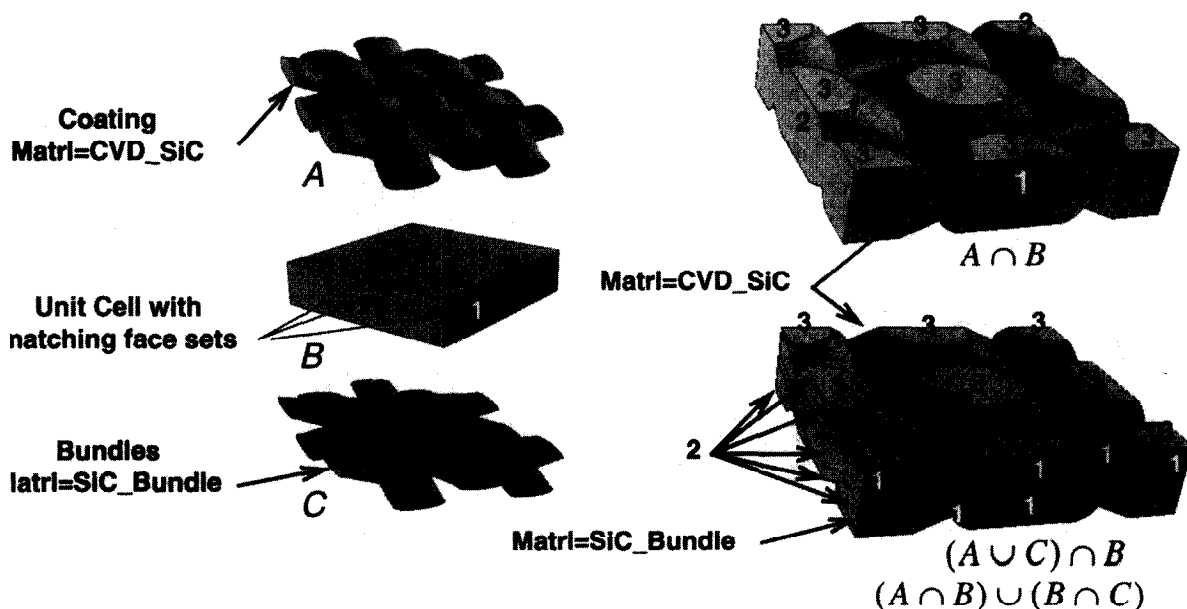


Fig. 11. Attribute propagation during model construction.

topological entity originally associated with a feature, and a set of precedence functions for the ancestor tags are installed with the basic operations underlying primitive creation, Boolean and sweep operations of the geometric modeler. The basic topological operations are: instantiate, copy, sweep, split, imbed and merge, as well as I/O for file storage. In the general case, basic operations can create a set of candidate topological entities whenever two topological entities are combined. An ancestor tag is propagated to newly constructed topological entities if it has precedence (a value less than) the tags of other topological candidates. The computational and memory cost rise linearly with model complexity.

The ancestor values can be assigned directly to an entity, such as to the solid region of a bundle, to multiple adjacent regions by a ‘locally greedy’ map coloring algorithm, or to related topological entities, such as the n th dimensional boundaries of an object or the common boundaries shared by two or more objects.

The unique identification of physical attributes are handled as a tuple: {geometric_entity, ancestor, attribute_type, attribute_label}. As the geometry of a new feature is processed, its corresponding attribute identification tuples are added to a database. When the model construction is completed, relational queries select tuples, evaluate them on the topology and return the set of matching topological entities, e.g. in Fig. 11 the set of faces on the RVE with attribute_type = ‘periodic_match’, and attribute_label = ‘3’. The matching entity set and other attribute data can be combined and formatted for later attribute processing.

In cases where there are competing propagation streams which must remain independent throughout the modeling process, a vector of ancestor tags is needed for each topological entity. This is analogous to the problem of multiple design ‘viewpoints’ for the topology of a part as described in [23,44], where each ancestor component corresponds to a viewpoint and is propagated independently.

Facilities for coordinating geometric information between the next lower and higher scales also makes use of the attribute propagation facilities. In the case homogenization of woven architectures, the linkage between scales is through non-isotropic material properties, and the modeling code provides inter-scale transformation topological entities to orient the properties of the lower scale along the length of the fiber bundles. The inter-scale transformation operator used by the automatic matched mesh generator is supplied the model, material region of interest, and location in space of an element integration point, and provides the corresponding orientation parallel to the bundle center line. Fig. 12 depicts the solid model of a weave (left) and the corresponding bundle path model (right), where the connection between entities of each model are by a common ancestor attribute. The path model in Fig. 12 is based on the partial design schematic of Fig. 8, the solid model has a meshed unit cell shown in Fig. 15(b), and the results are shown in Fig. 20. The same inter-scale transformation capabilities can be used to orient the mesoscale properties in a curved macroscale component, e.g. a mid-thickness surface can orient material properties in a shell component or delineate the extent of fabric layers.

3.3. Automatic matched meshing

The generation of valid finite element meshes [37,33] within the problem domain is critical to the success of these analyses. The topological and geometrical complexity of three-dimensional woven composite unit cells, and the need to analyze multiple unit cell models to optimize microstructure for a given application make the

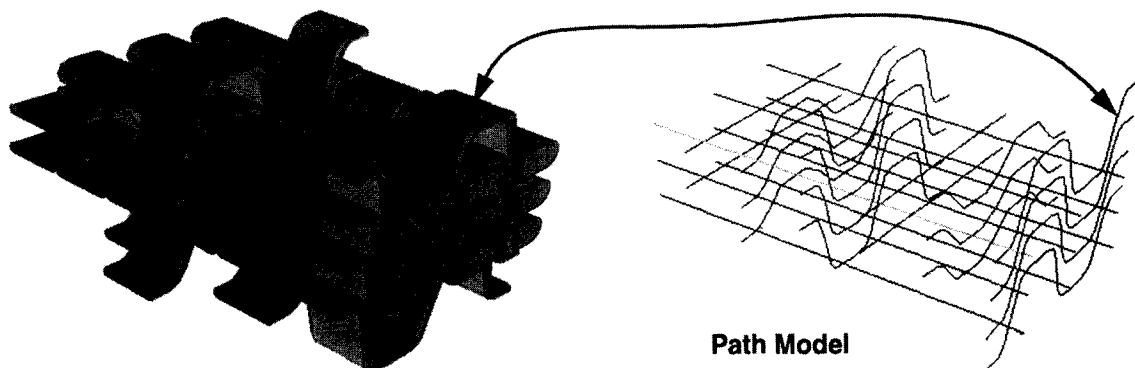


Fig. 12. Bundles and corresponding path model for fiber property orientation.

ability to generate meshes without user intervention a practical necessity. Operations associated with mesh generation for unit cell models are depicted in Fig. 13, where the geometric model and associated attributes are shown as inputs and the output is a data set formatted for the FE solver.

The schematic in Fig. 13 depicts the inputs and outputs (lines) for each function (boxes) used to implement the automated homogenization ‘Matched mesh model generation’ function of Fig. 4. The ‘Geometric Modeler’ provides a non-manifold boundary representation [26] of the composite weave geometry comprising the unit cell.

The ‘Matched Mesher’ function uses the geometric model information and constraints dictated by the periodic boundary conditions to automatically create a three-dimensional mesh of the composite weave. A set of ‘Mesh Copy Operations’ is used to create matching surface mesh topology and geometry on opposing faces of the unit cell. The mesh matching requirements, ‘Unit Cell Template’, is information to be associated with the previously attributed unit cell faces and are independent of any particular composite weave geometric model. The unit cell template information is associated with the topology of the unit cell template by the ‘Classify on Unit Cell’ function. After the mesh has been generated, mesh queries and manipulations are performed via the ‘Generic Mesh Database Operations’ [3].

The unit cell template is also used to automatically ‘Identify Moveable Constituent Topology’, as indicated in the center of Fig. 13. This function determines the topological entities of the given ‘Target Constituents’ in the composite weave model for which the associated mesh may be altered to ‘Adjust Constituent Mesh Volumes’ to the given ‘Target Volume Fractions’ by the subsequent function shown.

The ‘Material Property’ function of Fig. 13 produces the constitutive relations for each constituent in the composite. The necessary constituent material properties are selected from a relational material property database indexed by compound, form, manufacturer, environment, or other factors. Alternatively, the properties

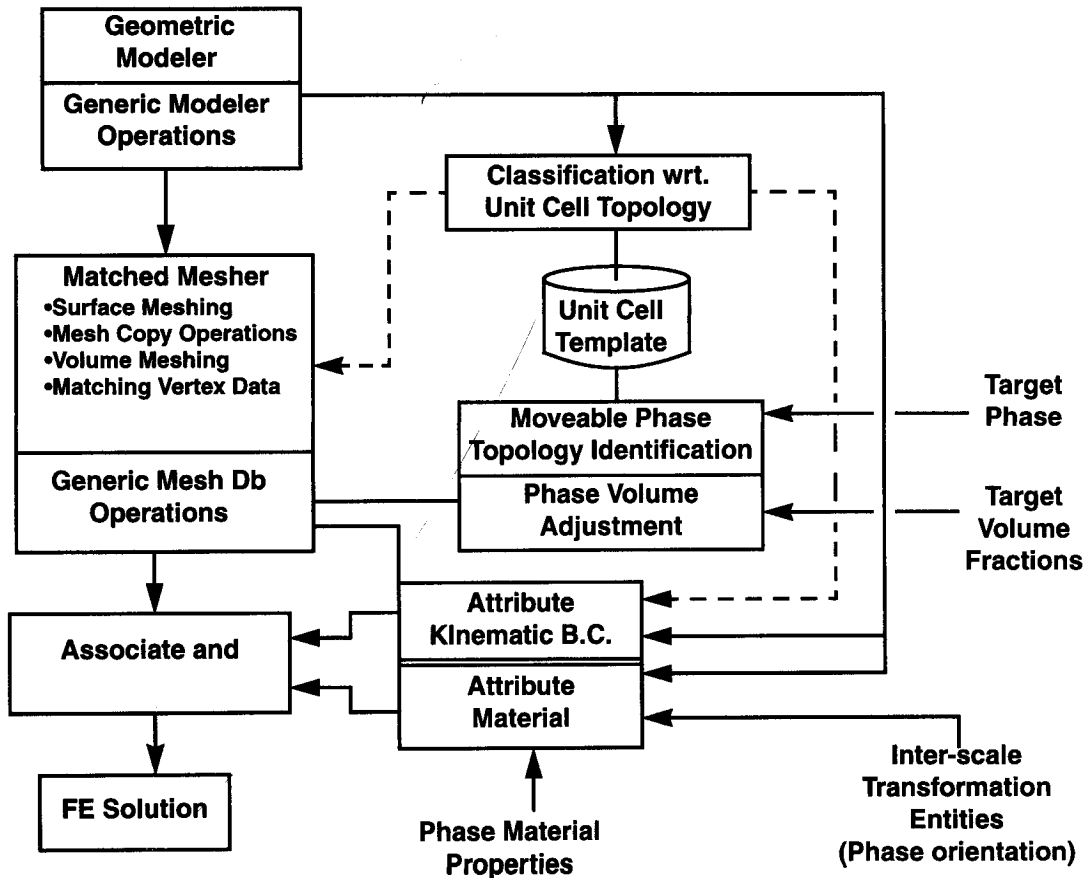


Fig. 13. Mesh related operations.

are computed from a lower scale analysis of the average properties of micro-constituents. Complete definition of material properties also requires the inter-scale transformation linkages described earlier to provide local coordinate systems orientation of non-isotropic material models. Data from the geometric modeler is used to associate the material properties (and other analysis attributes [4]) with the geometric model topology. Associating these properties with the geometric model makes them independent of the mesh, and the mesh can therefore be altered without requiring their re-specification.

The ‘Kinematic B.C. Attributes’ function of Fig. 13 defines the appropriate boundary conditions for the homogenization analysis. These attributes and the constitutive relations are associated with the correct finite element mesh entities and formatted as necessary for the finite element solver by the ‘Associate and Format’. The resulting system of equations is provided to the finite element solver, and the solution data is supplied to appropriate post processing routines.

3.4. Matched mesh generation

Since the homogenization modeling is performed via the finite element method, the necessary periodic boundary conditions are specified to the equation solver in terms of nodal displacement requirements (multi-point constraints). Since the displacement solution field is not constant over a cell face, the displacement of a given node, referred to as the subordinate node, on one face of the unit cell is defined as a function of the displacements of specific nodes, referred to as control nodes, on the opposing unit cell face. That is

$$\underline{u}_i = \sum_{j=1}^{N_{\text{con}}} a_j \underline{u}_j$$

where \underline{u}_i denotes the displacements of the i th subordinate node, \underline{u}_j denotes the displacements of the j th control node, a_j are weighting values, and N_{con} is the number of control nodes associated with the current subordinate node, see Fig. 14. The displacement function for a given node is written in terms of the shape functions of the element face which contains the projection of the given node on the opposing unit cell face. If it were implemented directly, this approach would require an expensive search process to determine within which element faces the projected node lies. The projected point must also be located in the parametric (ξ_1, ξ_2, ξ_3) space of the element face to express the displacement of the subordinate node in terms of the control nodes. The calculation is more complex with higher order polynomial element geometry interpolations. The computational penalty of the search also increases with high surface area to volume ratios of the unit cell, a condition found in many typical weaves, such as those shown in Fig. 15.

Specification of the periodic boundary conditions is simplified if the finite element nodes on opposing unit cell faces match ($N_{\text{con}} = 1$). Given a priori knowledge of the correspondence between nodes on opposing faces of the unit cell, no searching is required and it is not necessary to locate a projected point in real space within the parametric space of an element face.

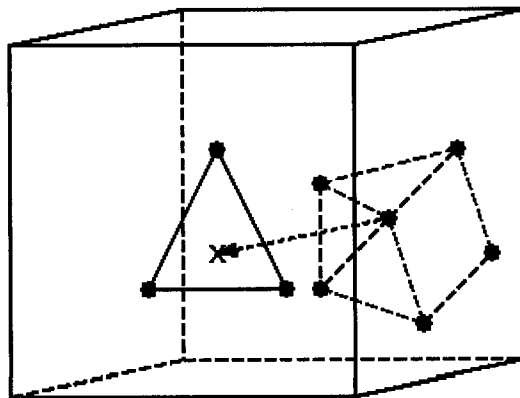


Fig. 14. Projection of a subordinate node onto its matching face and its surrounding control nodes.

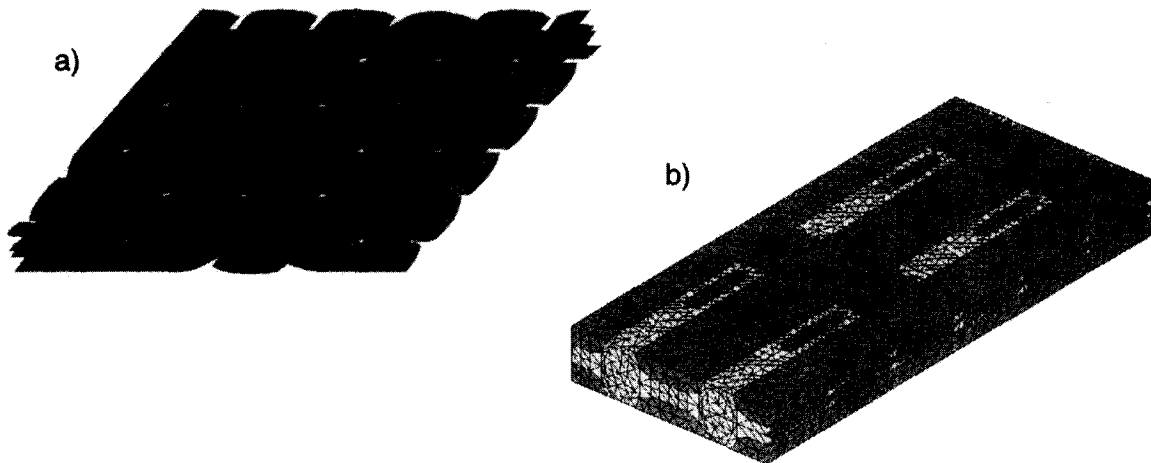


Fig. 15. Example bundle and unit cells meshes of a 5-harness and angle interlock weave.

Matched meshes are generated by discretizing the weave geometric model outer boundary entities which are defined as ‘control’ entities, and then copying the meshes to the matching ‘subordinate’ weave geometric model entities. To generate a matched mesh of the weave geometric model, it is necessary to identify the control–subordinate relationships of the weave geometric model outer boundary topological entities. For convenience, the outer boundary of the weave geometric model is denoted as δM , and the control–subordinate relationships are determined by associating the topological entities δM with the unit cell template control and subordinate topology.

One unit cell template face of each opposing pair of faces is specified as the control face, and the other is specified as the subordinate face. One of the three such pairs of faces is indicated on the unit cell template shown in Fig. 16(a). Periodicity in each direction normal to the faces of the unit cell requires that parallel edges of the box-shaped unit cell template undergo the same variations in displacement and must have identical meshes. One unit cell template edge in each group of four parallel edges is specified as the control edge, and the other three are designated as subordinate edges. One of the three such control–subordinate edge groups is shown in Fig. 16(a). All eight vertices of the unit cell undergo the same displacement, and (trivially) must have identical meshes.

Each δM face associated with a control face of the unit cell template is identified as a control face, and the matching δM face is identified as a subordinate face, as shown for a typical pair of weave geometric model faces

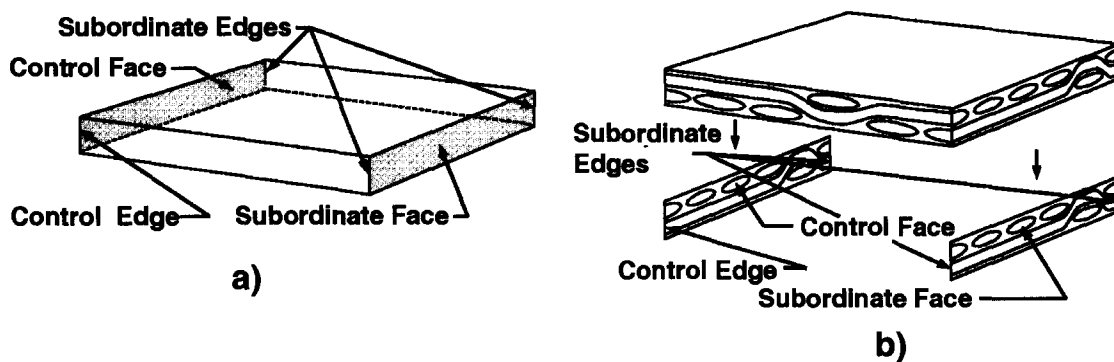


Fig. 16. Control–subordinate relationships of unit cell geometries.

in Fig. 16(b). If a δM edge lies within a control face of the unit cell template, then it has one matching δM edge lying within the opposing subordinate face of the unit cell template. If a δM edge lies on a control edge of the unit cell template, it has three matching edges lying on the parallel subordinate edges of the unit cell template, as shown for one group of δM edges in Fig. 16(b). The δM vertices similarly inherit control–subordinate designations.

Generating meshes in a hierarchic manner, i.e. meshing vertices first, then edges, faces, and volumes, allows the periodicity requirements to be easily satisfied during the meshing process, since discretizing the weave geometric model face boundaries first ensures that the necessary matching meshes can be generated in their adjacent faces.

The control δM edges are meshed, as shown in Fig. 17(a). As described in [10], the edge meshing is done such that the resulting discrete edges are of approximately the same size as initially requested. The meshes on the control edges are copied to the subordinate weave edges, after first creating a new subordinate mesh vertex as shown in Fig. 17(b). A new mesh edge is then created and classified on the subordinate weave edge, as shown in Fig. 17(c).

The weave faces are then meshed by a surface meshing algorithm which discretizes the model faces in their parametric spaces [10]. The weave face boundary mesh is first copied into the parametric space, as shown in Fig. 18(a), and the surface mesh is then created using a Delaunay insertion method [10], Fig. 18(b). After the surface mesh has been created in the parametric space it is copied back to the weave face in the real space by obtaining the corresponding xyz coordinates for each of the mesh vertex parameter values as shown in Fig. 18(c). The matching mesh on the subordinate weave face is created by copying the temporary mesh to the corresponding subordinate weave face.

The region meshing process is comprised of three steps [10]. In the first step an underlying variable level

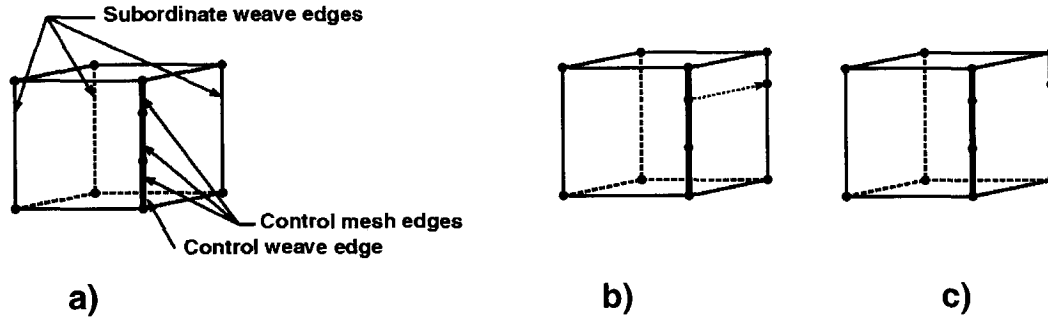


Fig. 17. Edge meshing procedure.

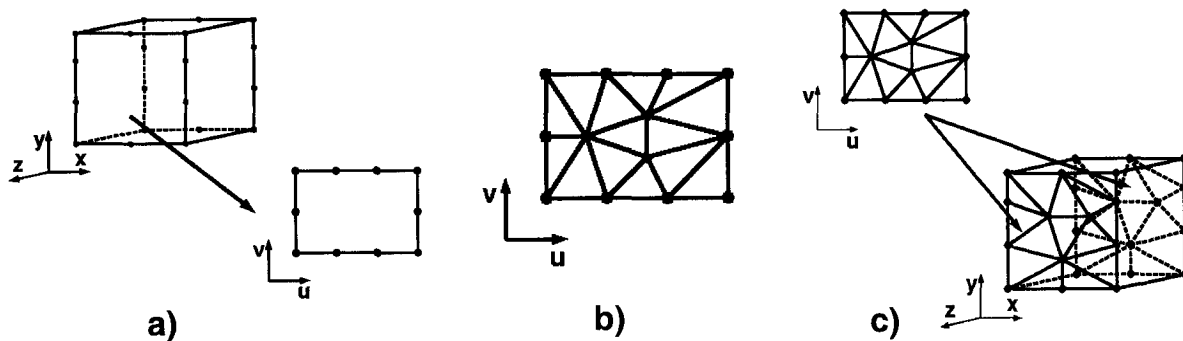


Fig. 18. Face meshing procedure.

octree is created to reflect mesh size control information during the region meshing procedure. The octants residing far enough inside the model interior are then meshed using templates. Finally, a face removal procedure connects the surface triangulation to the interior elements.

3.5. Control of constituent volume fractions

Given knowledge of the desired goal of the analysis, the modeling process can be adjusted for greater efficiency. In finite element analyses the solution accuracy is affected by both discretization error and geometric approximation error. If discretization error dominates, then the discretization must be suitably refined to improve solution accuracy. Geometric approximation error is caused by the piecewise approximation of curved model geometry. Since the fiber bundles are convex in cross-section and are curved to form the weave, geometric approximation creates errors in the constituent volume fractions calculated from the finite element mesh. A comparison of the discretization and geometric approximation errors for the 5-harness satin weave of Fig. 7(a) are shown in Fig. 19, where the percent error on the first three diagonal stiffness terms (G_{11} , G_{22} , G_{33}) are plotted for the independent cases of increasing refinement and three volume fraction errors (0%, 5%, 19.5%). An order of magnitude increase in the number of unknowns accounts for only a 2% error, while an error in volume fraction of less than 20% causes approximately 8% error.

The volume fraction errors are controlled by mesh modification, where the mesh vertices classified on the interior surfaces of the target constituents are relocated anisotropically, if necessary. In the current implementation, the quality of the mesh is maintained with respect to the largest dihedral angle [22] and a constrained Laplacian smoothing [12] is employed to improve the shapes of the altered elements [9].

3.6. Post processing

Stresses on the scale of the weave constituents aid in the design of composite microstructure by indicating areas of high stress which may lead to failure. Since the meshes generated here conform to the model geometry,

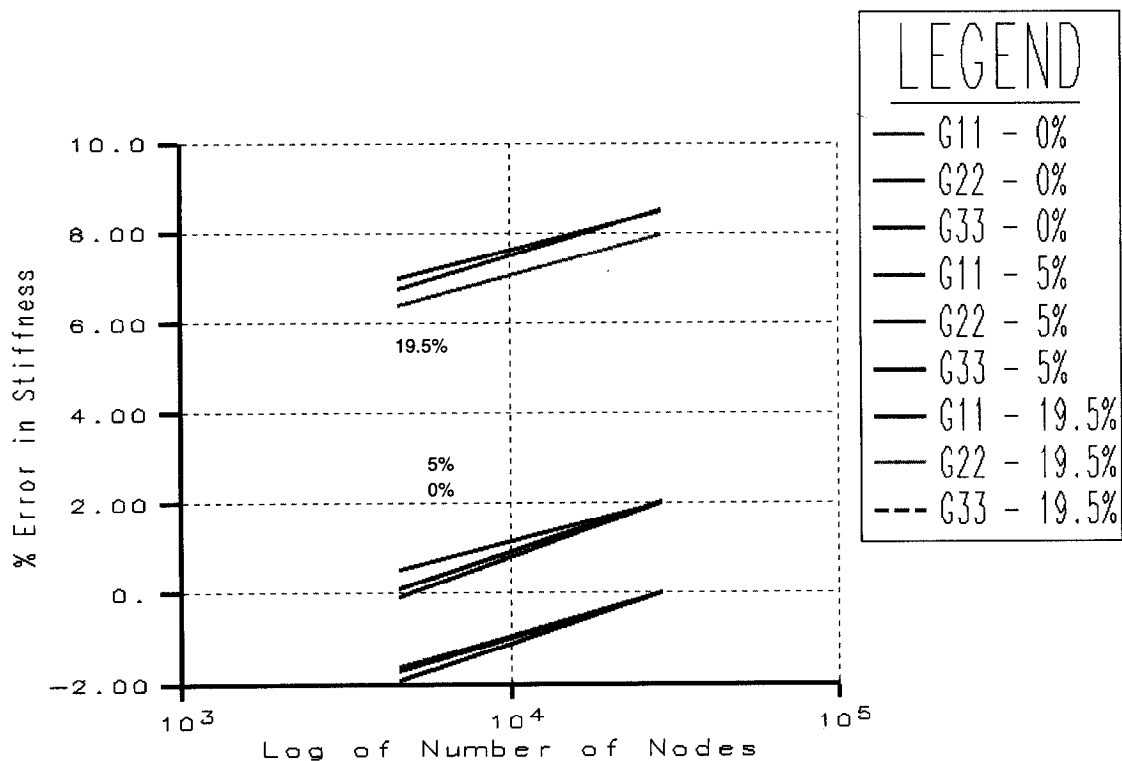


Fig. 19. Effect of discretization and geometric approximation error on homogenized stiffness.

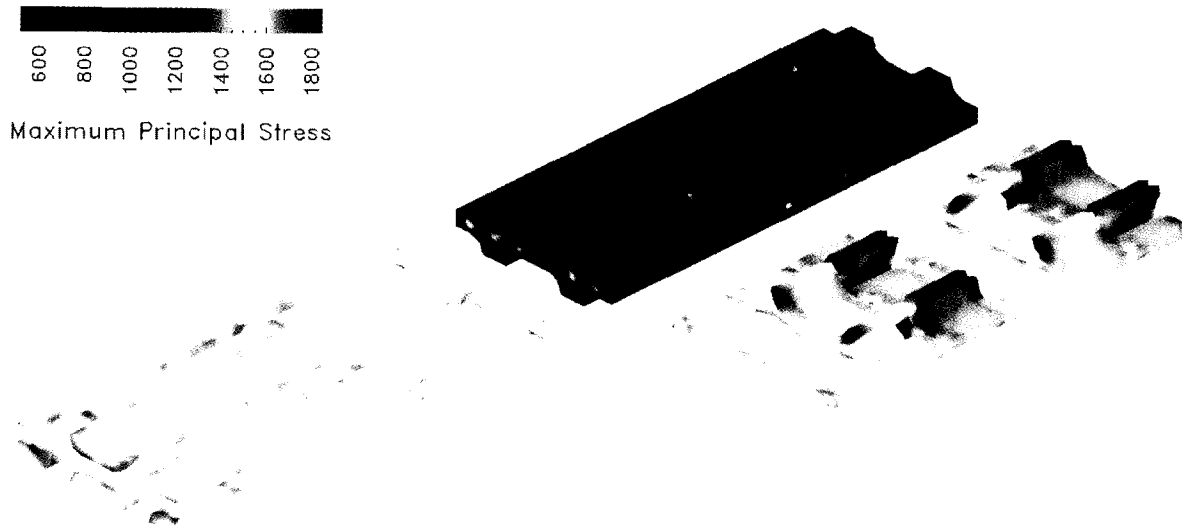


Fig. 20. Maximum principal meso scale stresses due to a 100 ksi uniform macro scale stress.

they can provide reliable local stress evaluation. The local unit cell stresses corresponding to the strain field $\hat{\epsilon}_j$ existing at a given j th point in the macroscale model are given by $\underline{\sigma}_i = \mathbf{B}_i^{\text{meso}} \hat{\epsilon}_j$ where $\underline{\sigma}_i$ are the stresses at the i th integration point in the unit cell model, and \mathbf{B}^{meso} is the stress concentration matrix relating the strain field at a given point in the macroscopic model to the stresses at the i th integration point in the unit cell model [13]. Implementation involves access to both macro and microscale solutions, access and transformations w.r.t. bundle path orientations, and tensorial computations. Consideration of the data flow indicated a potential combinatorial explosion of macro/mesoscale data, since macro scale finite element models contained 10^3 – 10^4 locations when both surface and thickness integration points are considered, and meso scale models contained 10^4 – 10^6 locations. The implementation was structured to minimize computations and also allowed unlikely combinations to be filtered out in the search for worst case values. Post processing capability was also extended to compute spectral norms of \mathbf{B}^{meso} of the mesoscale model, allowing comparison of alternative weave designs without macro scale analysis.

The following example of local stress calculation uses the angle interlock composite unit cell of Fig. 15. The homogenized material stiffness parameters were used to calculate $\hat{\epsilon}$ corresponding to a 100 ksi uniaxial stress in the x (warp) direction. The results of applying the above procedure to every integration point in the coarse mesh are shown in Fig. 20.

This figure represents an exploded view of the unit cell, with the groups of elements comprising the matrix (top center), warp bundles (left), and weft bundles (right) separated for clarity. Linear elements were used for the homogenization analysis of this example, and are colored according to the values of the maximum principal stress calculated at their single integration points. The correspondence between the colors and the stress values is shown by the grey scale at the top of the figure.

The stresses in the warp bundles show concentration ‘bands’ near the crossovers where the warp and weft bundles are woven together. This is due to the load carrying capacity of bundles being reduced when their axes do not align with the loading direction, and the load therefore being transferred to the neighboring bundles which are aligned in the loading direction. The matrix material shows bands of stress values due to additional reinforcement by the transverse stiffness of the weft bundles.

4. Conclusions

This paper presented tools used for efficient three-dimensional modeling and homogenization analyses of complex composite materials. The tools and techniques were presented to extract available material data from

test micrographs, compute non-manifold geometric models from a description of its features and known weave schematics and parameters, and facilities to assign and maintain attributes associated with topological entities for subsequent analysis. The ability to track attributes throughout the model construction process and to link geometry representing different scales are useful capabilities for automatic modeling in this application. A matched meshing algorithm was also presented, which simplifies the specification of periodic boundary conditions. An algorithm developed to correct the mesh volume fraction was used to study the effect of the mesh volume fraction error on the values of homogenized material stiffness parameters, and these errors were shown to be greater than that of the discretization error alone. Acceptable homogenization results may therefore be obtained with coarse discretization if the mesh volume fraction is controlled. The reliable calculation of local stresses due to loading on a macroscale domain was also demonstrated as a post-processing step for problems which are within the assumptions for uncoupled (homogenization) analysis. Such capability requires a mesoscale mesh which conforms to the model geometry and efficient processing of the woven solution data.

Acknowledgments

The support of ARPA/ONR under grant number N00014-92J-1779, and of the Allison Advanced Development Company under the LC³ project is gratefully acknowledged.

References

- [1] Adobe Inc., Adobe PhotoShop 3.0 User Guide, Adobe Systems, Inc., 1585 Charleston, P.O. Box 7900, Mountain View, CA, 94039-7900, USA, 1994.
- [2] N.S. Bakhvalov and G.P. Panasenko, *Homogenization: Averaging Processes in Periodic Media* (Kluwer Academic Publishers, 1989).
- [3] M.W. Beall and M.S. Shephard, A general topology-based mesh data structure, *Int. J. Numer. Methods Engrg.* 40(9) (1996) 1573–1596.
- [4] M.W. Beall and M.S. Shephard, A geometry-based analysis framework, *Advances in Computational Engineering Science* (Tech. Science Press, Forsyth, GA, 1997) 557–562.
- [5] Behrooz–Hassani, A direct method to derive the boundary conditions of the homogenization equation for symmetric cells, *Comm. Numer. Methods Engrg.* 12 (1996) 185–196.
- [6] L. Boatto, V. Consorti, M. Del Buono, S. Di Zenzo, V. Ermano, A. Esposito, F. Melcarne, M. Meucci, A. Morelli, M. Mosciatti, S. Scarsi and M. Tucci, An interpretation system for land register maps, *Computer* 25(7), July (1992) 25–33.
- [7] J. Bradley, XV – Version 3.0 Rev: 3/30/93, Shareware, 1053 Floyd Terrace, Bryn Mawr, PA, 19010.
- [8] A. Dasgupta, R.K. Agarwal, S.M. Bhandarkar, Three dimensional modeling of woven-fabric composites for effective thermo-mechanical and thermal properties, *Composite Sci. Technol.* 56 (1996) 209–223.
- [9] R. Collar, R. Wentorf, M.S. Shephard and J. Fish, Automated analysis of three-dimensional composite unit cells, *IJNME* (1997) submitted.
- [10] H.L. De Cougny, and M.S. Shephard, Surface meshing using vertex insertion, *Proc. 5th Int. Meshing Roundtable*, Report SAND96-2301, Sandia Corp., pp. 243–256, 1996.
- [11] M. Dohmen, A survey of constraint satisfaction techniques for geometric modeling, *Comput. Graph.* 19(6) (1995) 831–845.
- [12] D.A. Field, Laplacian smoothing and Delaunay triangulations, *Comm. Appl. Numer. Methods* 4 (1987) 709–712.
- [13] J. Fish and A. Wagiman, Multiscale finite element method for a locally non-periodic heterogeneous medium, *Comput. Mech.* 12 (1993) 164–180.
- [14] J. Fish and V. Belsky, Multigrid method for a periodic heterogeneous medium. Part I: Convergence studies for one-dimensional case, *Comput. Methods Appl. Mech. Engrg.* 126 (1995) 1–16.
- [15] J. Fish, V. Belsky, Multi-grid method for a periodic heterogeneous media, Part 2. Multiscale modeling and quality control in multidimensional case, *Comput. Methods Appl. Mech. Engrg.* 126 (1995) 17–38.
- [16] J. Fish, P. Nayak and M.H. Holmes, Microscale reduction error indicators and estimators for periodic heterogeneous medium, *Comput. Mech.: The Int. J.* 14 (1994) 1–16.
- [17] J. Fish, A. Suvorov and V. Belsky, Automated adaptive multilevel solver, *Comput. Methods Appl. Mech. Engrg.* 149 (1997) 267–297.
- [18] J. Fish and V. Belsky, Generalized aggregation multilevel solver, *Int. J. Numer. Methods Engrg.* 40 (1997) 4341–4361.
- [19] J. Fish and K.L. Shek, Finite deformation plasticity for composite structures: computational models and adaptive strategies, *Comp. Methods Appl. Mech. Engrg.* (1998) to appear.
- [20] S.J. Hollister and N. Kikuchi, A comparison of homogenization and standard mechanical analysis for periodic porous composites, *Comput. Mech.* 10 (1992) 73–95.
- [21] S.J. Hollister and N. Kikuchi, Homogenization theory and digital emaging: A basis for studying the mechanics and design principles for bone tissue, *Biotechnol. Bioeng.* 43 (1994) 586–596.

- [22] M. Krizek, On the maximal angle condition for linear tetrahedral elements, *SIAM J. Numer. Anal.* 29 (1994) 513–520.
- [23] E.C. Libardi, J.R. Dixon and M.K. Simmons, Computer environments for the design of mechanical assemblies: A research review, *Engrg. Comput.* 3 (1988) 121–136.
- [24] L. Lam, S.-W. Lee and C.Y. Suen, Thinning methodologies—A comprehensive survey, *IEEE Trans. Pattern Anal. Machine Intelligence* 14(9) (1992) 869–885.
- [25] P. Lipetzky, N.S. Stoloff and G.J. Dvorak, Atmospheric effects on high temperature lifetime of ceramic composites, in: *Ceramic Engineering and Science Proceedings*, Vol. 18, Issue 4, 21st Annual Cocoa Beach Conference on Composites, Advanced Ceramics, Materials and Structures—B, American Ceramic Society, Cocoa Beach, FL, pp. 1997.
- [26] M. Mantyla, *Introduction to solid modeling* (Computer Science Press, Rockville, MD, 1988).
- [27] C.C. Mei and J.L. Auriault, Mechanics of heterogeneous porous media with several spatial scales, *Proc. R. Soc. Lond., A* 426 (1989) 391–423.
- [28] T. Mori and K. Tanaka, Average stress in matrix and average elastic energy of materials with misfitting inclusions, *Acta Metall.* 21 (1973) 571–574.
- [29] F. Noubound and R. Plamondon, On-line recognition of handprinted characters: Survey and beta tests, *Pattern Recogn.* 23(9) (1990) 1031–1044.
- [30] J.T. Oden and T.I. Zohdi, Analysis and adaptive modeling of highly heterogeneous elastic structures, TICAM report, December 1996.
- [31] L. O’Gorman and R. Kasturi, Chapter 3, Feature Level Analysis, *Document Image Analysis* (IEEE Computer Society Press, Los Alamitos, CA, 1995).
- [32] R. Pandey, and H.T. Hahn, Visualization of representative volume elements for three-dimensional four-step braided composites, *Composites Sci. Technol.* 57 (1997) 703–713.
- [33] W.J. Schroeder, Geometric triangulations: With application to fully automatic 3D mesh generation, Ph.D. Thesis, Rensselaer Polytechnic Institute, Scientific Computational Research Center, RPI, Troy, NY, 12180-3590, May 1991, SCOREC Report # 9-1991.
- [34] B.V. Sankar and R.V. Marrey, Analytical method for micromechanics of textile composites, *Composites Sci. Technol.* 56 (1996) 161–170.
- [35] J. Shah, Conceptual development of form features and feature modelers, *Res. Engrg. Des.* 2(2) (1991) 93–108.
- [36] M.S. Shephard, The specification of physical attribute information for engineering analysis, *Engrg. Comput.* 4 (1988) 145–155.
- [37] M.S. Shephard and M.K. Georges, Reliability of automatic 3-D mesh generation, *Comput. Methods Appl. Mech. Engrg.* 101 (1992) 443–462.
- [38] P. Tong and C.C. Mey, Mechanics of composites of multiple scales, *Comput. Mech.* 9 (1992) 195–210.
- [39] D. Wildman, J. Schwefel and J. Chang, Allison Engine Co., Photo-micrographs of ceramic/ceramic high temperature composite material, 1996.
- [40] J. Whitcomb, K. Srengan and C. Chapman, Evaluation of homogenization for global/local stress analysis of textile composites, *Composite Struct.* 31 (1995) 137–149.
- [41] K.J. Weiler, The radial-edge structure: A topological representation for non-manifold geometric boundary representations, in: M.J. Wozny, H.W. McLaughlin and J.L. Encarnacao, eds., *Geometry for CAD Applications* (North Holland, 1988) 3–36.
- [42] K.J. Weiler, Topological structures for geometric modeling, Ph.D. Thesis, Rensselaer Design Research Center, Rensselaer Polytechnic Institute, Troy, NY, May, 1986.
- [43] R. Wentorf, M.S. Shephard, E.V. Korngold, The use of functional models to control engineering idealizations, *Proc. 1989 ASME International Computers in Engineering Conference and Exposition*, Anaheim, CA, July, 63–70.
- [44] XOX Corp., SHAPES Kernel: A System For Computing with Geometric Objects, Reference Manual, XOX Corp., 1450 Energy Park Drive, Suite 120, St. Paul, MN, 55108, USA, 1995.